The 8th European Congress on Computational Methods in Applied Sciences and Engineering
ECCOMAS Congress 2022
5-–9 June 2022, Oslo, Norway

LES-AIDED SHAPE OPTIMISATION OF U-BEND CHANNEL

Russell Quadros[1], Lionel Cheng[2], Gabriel Staffelbach[2], Mladen Banović[3], Arthur Stück[3] and Jens-D. Müller[1]

[1] Queen Mary University of London
Mile End Rd, Bethnal Green
email: r.quadros@qmul.ac.uk London E1 4NS

[2] Centre Européen de Recherche et de Formation Avancée en Calcul Scientifique (CERFACS)
42 Av. Gaspard Coriolis
31100 Toulouse, France

[3] Deutschen Zentrum für Luft- und Raumfahrt (DLR)
Zwickauer Strasse 46
01069 Dresden

Key words: shape optimisation, adjoint, large-eddy simulation, Reynolds-averaged Navier-Stokes simulation

Abstract. Reynolds-Averaged Navier-Stokes (RANS) simulations are inaccurate in predicting complex flow features (ex: separation regions), and therefore deriving an optimised shape using the RANS-adjoint framework does not yield a truly optimal geometry. With the purpose of obtaining accurate sensitivity to objective function of interest, we improve the RANS flowfield using the strategy of Singh et al. [1]. This involves multiplying a corrective factor β to the production term in the Spalart-Allmaras (SA) turbulence model equation and solving the inverse problem to determine the appropriate β field, which enables the RANS solution to match the high-fidelity data. The geometry of our interest is the U-Bend which is widely studied in literature in the context of gas turbine cooling, and which is known to be a challenging case for RANS simulations to reproduce. We use the mean flowfield from a large-eddy simulation of the U-Bend geometry as the high-fidelity data to which the RANS flowfield is fit using the β strategy outlined above. We observe a clear improvement in the RANS flowfield by optimising for the β field, the objective function to be minimized being L2-norm of the mean velocity difference between RANS and LES. We further show that adding an additional corrective factor (γ) to the destruction term in the SA turbulence equation and simultaneously optimising for the γ field alongside the β field results in a better match of the RANS flowfield with the corresponding LES flowfield. We also show that surface sensitivity map for the improved LES-aided flowfield varies significantly in comparison to the baseline SA-based flowfield for an objective function of interest, the total pressure loss in the U-Bend.

1 Introduction

Aerodynamic shape optimisation (ASO) modifies the bounding walls and affects the flow features with the aim to improve an objective function of interest (ex: lift, drag, etc). Adjoint methods are most effective in ASO through providing sensitivity of a given objective function w.r.t any number of input parameters at a near-constant cost [2] and are widely used in the Reynolds-averaged Navier-Stokes (RANS) framework. RANS models the turbulence in terms of mean flow variables and calibrated constants and largely relies on the eddy-viscosity hypothesis, which breaks down in complex flows, such as those involving severe separation. Therefore, the optimised shapes obtained in a RANS-adjoint framework for complex flows may not be truly optimal in nature. Large-eddy simulation (LES) resolves the larger turbulent eddies in the flow and models the small eddies in terms of mean flow variables, and is known to be more accurate than RANS. Since LES resolves the chaotic turbulent motions in the flow, the adjoint method cannot be used in conjunction with LES for shape optimisation since the gradients blow up and practical regularisation methods are not available [3].

Hayek [4] improved the RANS prediction in a U-Bend geometry by using a frozen-eddy viscosity approach, which involves optimising the eddy-viscosity (ν_t) field such that the RANS mean velocity matches the LES mean velocity. This ν_t-optimisation is driven by the adjoint method, which provides sensitivity of the objective function to the eddy viscosity at every mesh point in the computational domain. This strategy was further extended by Alessi et al. [5] who first obtained the eddy-viscosity field using the ν_t-optimisation outlined above, and then used the improved flowfield to carry out the shape optimisation of the VKI U-Bend geometry [7] by using a frozen ν_t approach [6]. They recomputed the LES after every design step, which indicates that while the LES flowfield can be matched with frozen turbulence, gradient accuracy is too poor for effective shape optimisation.

Singh et al. [1] used an alternate strategy to improve the RANS prediction. They multiplied the production term in the turbulence model equation with a factor β, and optimised the β field for all the mesh points in the computational domain so that the objective function matches the corresponding value in a higher fidelity model (either experiment or large-eddy simulation). They solved for the flow around airfoil and used adjoints to optimise the β field such that the lift coefficient (c_l) predicted by RANS would match the corresponding experimental value. They then modeled β in terms of local flow features (such as ratio of SA-production to SA-destruction), and trained a neural network on a large airfoil dataset for which the experimental data was available. The outcome was a framework that was capable of predicting the corrective β value based on the local flow features, and this neural network augmented SA model was applied to untrained datasets to show clear improvement in comparison to the base SA model prediction.

Although this procedure is suitable for cases where significant experimental data exists (ex: airfoils), generating a generalized β for non-conventional geometries is challenging. Recent advances in high-performance computing has enabled large-eddy simulation of complex geometries at fairly high Reynolds number [8]. Our goal is to use the β-fit strategy outlined above in conjunction with LES data to improve the RANS prediction, and employ the corrected flowfield to obtain better surface sensitivities towards shape optimisation. The adjoint sensitivities obtained through the β-fit strategy are more accurate (in comparison to the frozen ν_t approach)

as they involve differentiating the turbulence model, and therefore are more suitable towards shape optimisation.

For our study, we choose the U-Bend configuration representing the serpentine cooling channels found in gas turbines. This geometry has been extensively studied both experimentally [20] and numerically [7], and is a known test case where RANS fails [5]. Since the Reynolds number of the U-Bend flow is moderate ($\approx 40,000$), this test case is amenable to large-eddy simulation at a reasonable cost [4]. The sections in the paper are outlined as follows. The methodology for improving the RANS flowfield based on the β-fit strategy and the $\beta-\gamma$-fit strategy is discussed in section 2. The baseline U-Bend experimental results are compared with LES and RANS in section 3.1. The improved RANS flowfield solution using the β-fit strategy and the $\beta-\gamma$-fit strategy are discussed in sections 3.2. Implications of improving the RANS flowfield on the surface sensitivity are discussed in section 3.3. Finally, the key conclusions are described in section 4.

2 Methodology

2.1 LES-fit strategy

The SA turbulence model [17] is a one-equation model which is used to solve for turbulent flows by modelling the Reynolds stress in the RANS governing equations. The standard SA turbulence model has significant shortcomings especially in accurately predicting separated flows [1]. The modified SA turbulence model that accounts for system-rotation and streamline-curvature effects also lacks accuracy in predicting highly curved channels in comparison to high-fidelity simulations [18]. Following the strategy of [1], we introduce a spatially varying β factor which multiplies the production term in the SA differential equation,

$$\frac{D\tilde{\nu}}{Dt} = \beta(x)P(\tilde{\nu},\mathbf{U}) - \mathbf{D}(\tilde{\nu},\mathbf{U}) + \mathbf{T}(\tilde{\nu},\mathbf{U}), \tag{1}$$

where P, D and T represent the production, destruction and the transport of the eddy viscosity. The aim is to find out the optimal value of β at every mesh point in the computational domain so as to minimize the objective function, which in our work is the square of the L2-norm of the mean velocity difference between the LES and the RANS solution,

$$J = \sum_{i=1}^{N} \left(U_{i,\mathrm{RANS}} - U_{i,\mathrm{LES}} \right)^2. \tag{2}$$

The optimal β field is obtained by solving the adjoint problem to find out the gradient of the objective to β and optimise using the L-BFGS-B method in the Python Scipy optimizer.

In certain flow cases such as the U-Bend channel, using β-fit strategy alone may result in the optimiser generating spatially varying β values which are either very high or close to zero (See section 3.2). This is especially true in region of the flowfield where mean shear rate is small and β which multiplies this low mean shear rate is driven to extreme bounding values in order minimise the objective. As an alternate strategy to improve the RANS prediction, alongside β we also multiply the destruction term with a factor γ,

$$\frac{D\tilde{\nu}}{Dt} = \beta(x)P(\tilde{\nu},\mathbf{U}) - \gamma\mathbf{D}(\tilde{\nu},\mathbf{U}) + \mathbf{T}(\tilde{\nu},\mathbf{U}), \tag{3}$$

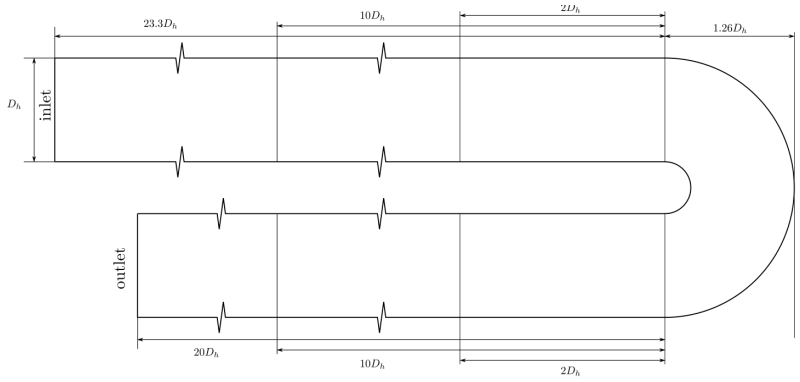

Figure 1: Dimensions of the U-Bend geometry as used in the experimental set up [9]

Variable	Value
Reynolds No.	43830
Inlet Bulk Velocity (m/s)	8.8
Inlet Turb. Intensity	5%
Density (Kg/m^3)	1.204
Inlet Temp. (K)	293.15
Molecular Visc. (kgs^{-1}m^{-}1)	1.813×10^{-5}
Outlet Pressure (Pa)	1.013×10^{5}

Table 1: Experimental conditions for the U-Bend geometry

and solve for optimal β and γ fields which cooperatively minimise the objective function provided in Eq. 2.

2.2 Test-case description

The U-Bend geometry as used in the experimental set up is shown in figure 1 and consists of a circular U-Bend profile with an inlet and an outlet leg. The channel has a height and width of 1 D_h (aspect ratio=1), and the inlet leg has a length of 23.3 D_h which ensures that the flow before the U-Bend is fully developed. Here, $D_h = 0.075\,m$ represents the hydraulic diameter. The experimental boundary conditions are provided in table 1. A detailed description pertaining to the geometry can be found in [9].

2.3 U-Bend Parameterisation

As mentioned in section 2.2, the U-bend geometry consists of a circular U-part with attached inlet and outlet legs. The parameterisation is done on the U-part, while the attached legs remain fixed during the optimisation. The U-part parameterisation is based on a cross-sectional design approach, which is also known as the *lofting* operation in the context of Computer Aided Design (CAD). This method constructs a three-dimensional (3-D) U-part shape by taking as input a number of rectangular two-dimensional (2-D) cross-sections (slices) constructed and distributed

uniformly along a guiding circular path-line. The path-line is defined as a B-spline curve and its parameters are fixed. The 2-D slice consists of four Bézier curves constructed on a plane that is orthogonal to the path-line and these curves are coupled as a closed wire having in total 12 control points.

The coordinates of each 2-D control point are not manipulated directly, but every control point has its own law of evolution along the path-line that determines its position on a specific plane. The laws of evolution are defined as 3-D B-spline curves, having eight control points each, where the first two and the last two control points are fixed to ensure the tangent continuity between the U-part and the attached legs. Finally, the (x, y) coordinates of the remaining four control points that are allowed to be moved are the actual design parameters considered in the optimisation. For this test-case, the total number of design parameters is 96 (12 laws of evolution $\cdot$ 4 control points per law of evolution $\cdot$ 2 coordinates per control point). The parameterisation code is written in C++ and it employs the classes from the open-source CAD kernel Open CASCADE Technology. A detailed description is available in [22].

2.4 Simulation Details

The LES is performed using the HPC code AVBP [10] developed at CERFACS. The Lax-Wendroff convective scheme which is second order accurate in time and space [11] and a 2Δ diffusion operator [12] are respectively used for the convective and diffusion terms. The WALE sub-grid scale model [21] developed for wall bounded flows is used for LES closure and artificial viscosity using the Colin model [12] is applied. The desired boundary conditions are obtained by employing a wall law [14] at each of the wall and a characteristic boundary condition (NSCBC) based on static pressure at the outlet [15]. Turbulence is injected with a Poiseuille profile at the inlet with a turbulence intensity of 5%. The numerical parameters used for the LES simulation are summarized in Tab. 2.

	Numerical parameters
Convection scheme	LW: $\mathcal{O}(2)$ in space and time [11]
Diffusion scheme	2Δ operator [12]
SGS model	WALE [21]
Artif. viscosity	Colin model: $\epsilon^{(2)} = 0.01$, $\epsilon^{(4)} = 0.005$ [12]

Table 2: Numerical parameters for the LES simulation

3 Results

3.1 LES of baseline U-Bend geometry

We compare the mean velocity field at the mid-plane ($z/D_h = 0.5$) as predicted by LES and RANS with the experiments [20] in figure 2. Both the experiment and the LES clearly capture the separation region after the flow turning, and the RANS simulation severely under-predicts the separation bubble. We show the turbulence kinetic energy (TKE) as predicted by the experiment [20] and the LES in figure 3. We observe a decent overall match in the TKE levels, except in the flow-separation region. The higher turbulence levels predicted by the LES

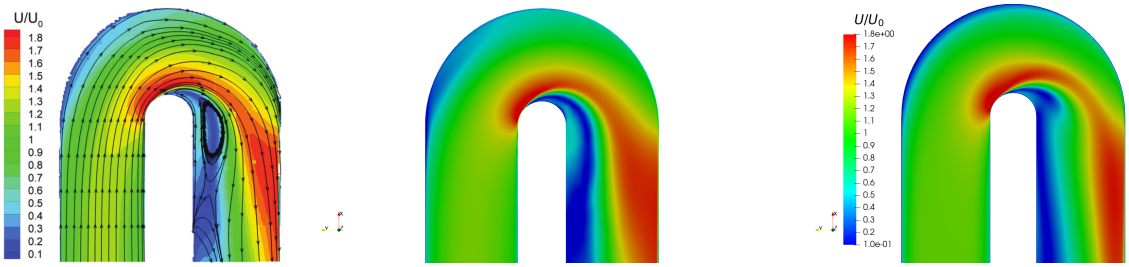

(a) Experiment (b) LES (c) RANS-SA

Figure 2: Mean velocity field at $z/D_h = 0.5$ as predicted by (a) experiment, (b) LES and (c) RANS-SA

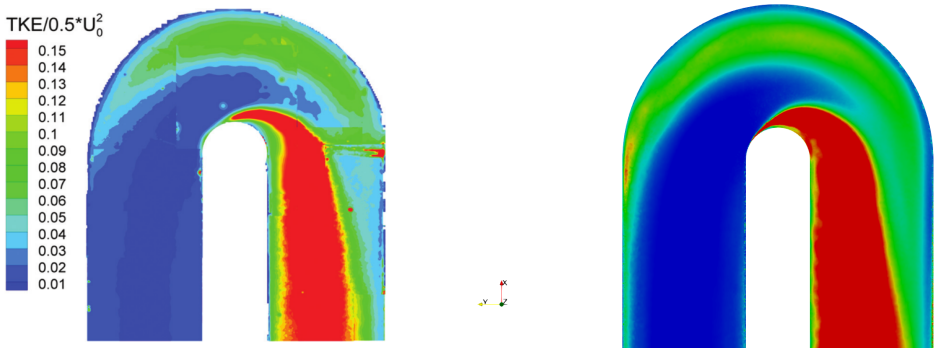

(a) Experiment (b) LES

Figure 3: Turbulence kinetic energy at $z/D_h = 0.5$ as predicted by (a) experiment, (b) LES

in this region probably indicates to a need for mesh refinement in order to capture the complex dynamics of the separation bubble accurately.

3.2 LES-fit RANS solution

In order to drive the RANS flowfield to match the LES, we employ two strategies discussed in section 2.1, namely the β-fit (Eq. 1) and the $\beta - \gamma$-fit (Eq 3) strategy. Figure 4 shows the convergence curve for the β-fit and the $\beta - \gamma$-fit optimisation highlighting the reduction in objective function described in Eq 2. We employ the Python Scipy optimiser to drive the optimisation using the L-BFGS-B method. We observe a clear advantage in the $\beta - \gamma$ strategy in comparion to the β-fit both in terms of a faster convergence to optimal value and a lower final value of the objective function.

The mean velocity at the mid-plane ($z/D_h = 0.5$) for the optimised β and the $\beta - \gamma$-fit are shown in figures 5c and 5d, respectively. The mean velocity as predicted by the baseline SA model is also shown for reference (figure 5b). The field optimisation significantly changes the flow structure from the baseline case and aligns it much closer to LES mean velocity (figure 5a). We observe a clear improvement in the $\beta - \gamma$-fit in comparison to the β fit both in the

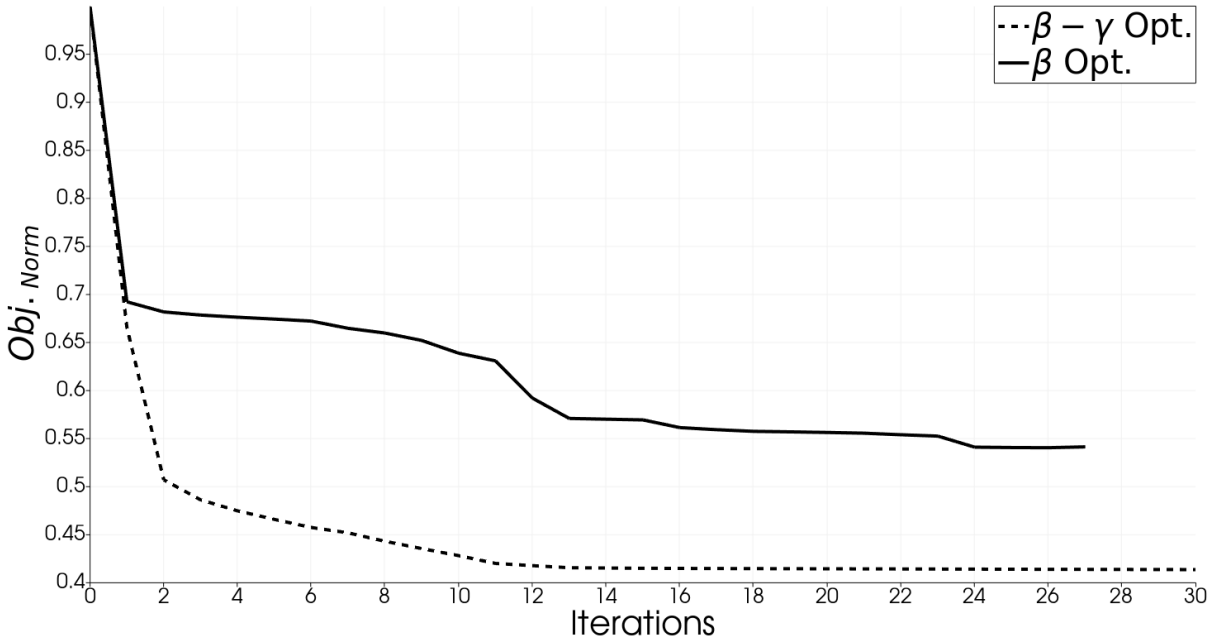

Figure 4: Objective convergence for β-fit and $\beta - \gamma$-fit optimisation

separation region after the flow turning, and the region close to the outer U-Bend surface, which is consistent with the greater drop in the $\beta - \gamma$-fit objective function seen in figure 4.

Although the objective function to minimise is the velocity difference between the LES and the RANS solution, both the β and the $\beta - \gamma$-fit show a distinct improvement in the pressure field as well. Figures 6c and 6d show the mean pressure at the mid-plane ($z/D_h = 0.5$) for the optimised β-fit and $\beta - \gamma$-fit cases, respectively. We observe a clear improvement from the mean pressure as predicted by the baseline SA (figure 6b), and the optimised fields are closer to the LES (figure 6a). Both the β and the $\beta - \gamma$-fit fail to reproduce the large low-pressure region post the U-turn observed in the LES, which can be better matched by considering the pressure difference between the LES and RANS in the objective function.

The optimised β map for the β-fit case and the optimised β and γ maps for $\beta - \gamma$-fit case at $z/D_h = 0.5$ are shown in figure 7. A contour line corresponding to a value of unity is also plotted in each of the maps. The β map corresponding to the β-fit case (figure 7a) shows several regions of low β value indicating an almost negligible value of ν_t production. A more uniform value of β is observed in the $\beta - \gamma$-fit case (figure 7b), the variation of which is also influenced by the γ map (figure 7c) corresponding to the ν_t destruction. We observe that several regions in the β map with increased β are complemented by a decreased γ in the same regions. Thus, both β and γ modifications work in tandem to minimise the objective function.

3.3 Implication of corrected RANS field on Surface Sensitivity

We use the improved flowfields obtained through the β and the $\beta - \gamma$-fit to study the surface sensitivity to an objective function of interest, the total pressure loss in the U-Bend channel,

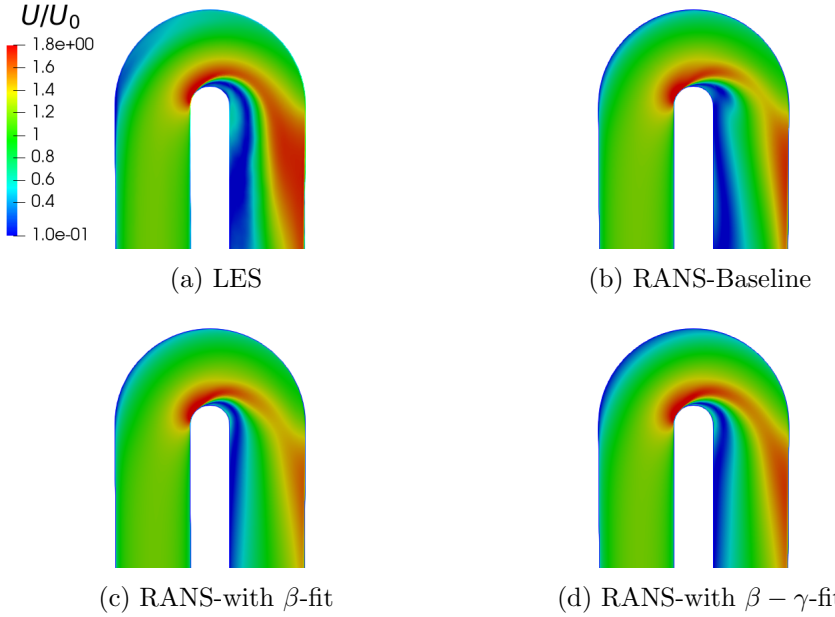

(a) LES (b) RANS-Baseline

(c) RANS-with β-fit (d) RANS-with $\beta - \gamma$-fit

Figure 5: Mean velocity at the mid-plane ($z/D_h = 0.5$) as predicted by (a) LES, (b) RANS, (c) β-fit RANS and (d) $\beta - \gamma$-fit RANS

which is defined as

$$J = \frac{\int_{inlet} p_{tot}(u \cdot n)dS - \int_{outlet} p_{tot}(u \cdot n)dS}{\int_{inlet}(u \cdot n)dS,}$$

where p_{tot} is the total pressure, u is the velocity vector, n is the normal direction and S is the cross-sectional area. Figure 8a shows the surface sensitivity to total pressure loss as obtained using the baseline SA model. In comparison to the SA-baseline value, the surface sensitivity for the improved flowfield obtained through the $\beta - \gamma$-fit (figure 8b) shows both a qualitative and quantitative difference. The relatively different surface sensitivity map in the $\beta - \gamma$-fit has a direct influence on the shape optimisation path and on the final optimal shape of the U-Bend. The surface sensitivity for the β-fit however has significantly higher values in the U-Bend region, and needs further investigation to determine the cause for these high values.

4 Conclusion

In this paper, we have presented a a detailed study of the benchmark VKI U-Bend test case using RANS and LES. We have shown the inability of RANS simulation in capturing the complex flow physics including the prominent separation region, which is well captured by LES. We have used two strategies to improve the RANS flowfield and match the RANS mean velocity to the LES mean velocity. The first strategy is the β-fit strategy based on the works of Singh et al. [1] which multiplies a β factor to the SA production term, and uses adjoint to optimise the β value at every grid point so as to minimise the mean velocity difference between the LES and the RANS simulation. The second strategy is the $\beta - \gamma$-fit, which in addition to modifying the production through a β factor, also optimises the γ factor which multiplies the

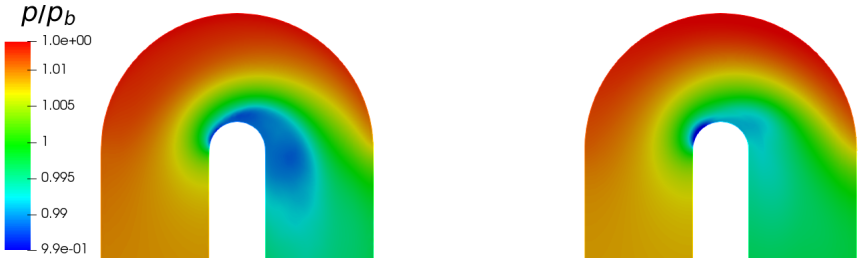

(a) LES (b) RANS-Baseline

(c) RANS-β-fit (d) RANS-$\beta-\gamma$-fit

Figure 6: Mean pressure at the mid-plane ($z/D_h = 0.5$) as predicted by (a) LES, (b) RANS, (c) β-fit RANS and (d) $\beta-\gamma$-fit RANS

SA destruction term. We have shown that the $\beta-\gamma$ strategy is more effective in yielding a better mean velocity fit to the LES as compared to the β-fit strategy. Although the objective function being minimised is the velocity difference, we have shown that the pressure field also improves significantly using these two strategies. We have further demonstrated that the surface sensitivity to an objective function of interest-the total pressure loss through the channel, varies both qualitatively and quantitatively for the improved RANS flowfield in comparison to the baseline SA model results. Using either of the two flow-improvement strategies outlined in this work in the shape-optimisation workflow can lead to a final LES-aided shape that is closer to the true optimal shape as compared to a pure RANS-based optimal shape.

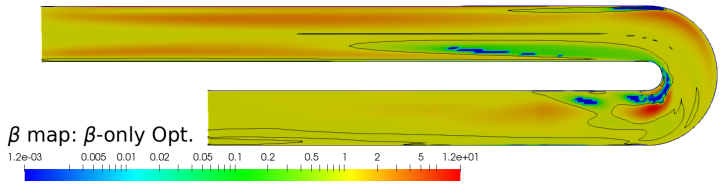

(a) β map for β-fit

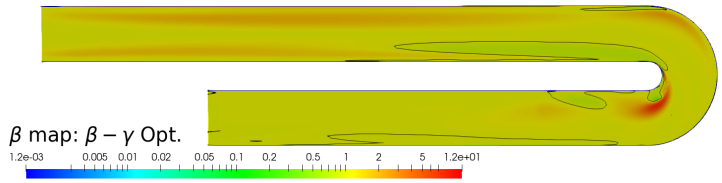

(b) β map for $\beta - \gamma$-fit

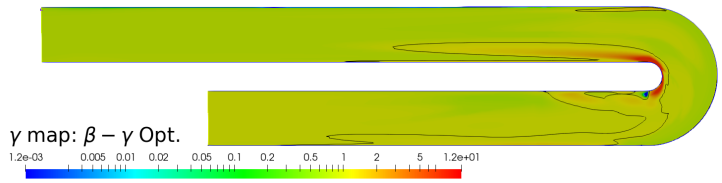

(c) γ map for $\beta - \gamma$-fit

Figure 7: Map of the converged correction factor for β-fit and $\beta - \gamma$-fit along with a contour line corresponding to a value of unity

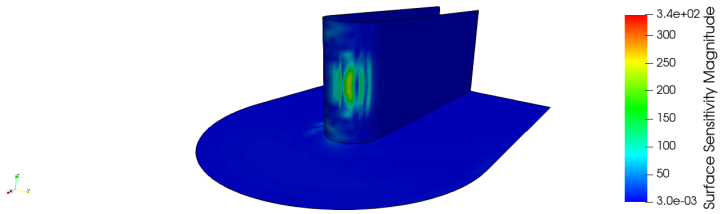

(a) SA-baseline

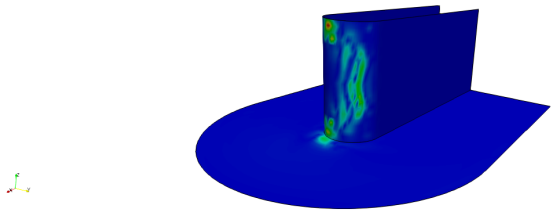

(b) $\beta - \gamma$-fit

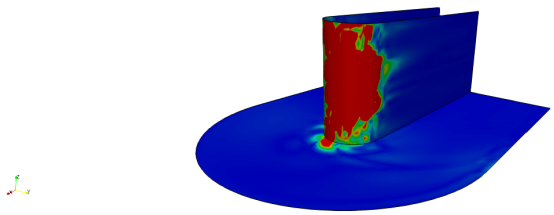

(c) β-fit

Figure 8: Surface sensitivity to the objective function, total pressure loss as predicted by SA-baseline, $\beta - \gamma$-fit SA model and β-fit SA model.

REFERENCES

[1] A. P. Singh and S. Medida and K. Duraisamy, Machine-Learning-Augmented Predictive Modeling of Turbulent Separated Flows over Airfoils, *AIAA Journal*, Vol. **55**, 2017.

[2] T. Verstraete and L. Müller and J. D, Müller, Adjoint-Based Design Optimisation of an Internal Cooling Channel U-Bend for Minimised Pressure Losses, *International Journal of Turbomachinery, Propulsion and Power*, Vol. **2**, 2017.

[3] J. Larsson and Q. Wang, The prospect of using large eddy and detached eddy simulations in engineering design, and the research required to get there, *Philosophical Transactions of the Royal Society A: Mathematical, Physical and Engineering Sciences*, Vol. **372**, 2014.

[4] M. E. Hayek, Adjoint-based optimization of U-bend channel flow using a multi-fidelity eddy viscosity turbulence model, *Masters Thesis, Massachusetts Institute of Technology. Department of Aeronautics and Astronautics.*, Vol. , 2017.

[5] G. Alessi and T. Verstraete and L. Koloszar and B. Blocken and J.P.A.J. van Beeck, Adjoint shape optimization coupled with LES-adapted RANS of a U-bend duct for pressure loss reduction, *Computers and Fluids*, Vol. **228**, 2021.

[6] M. Schramm and B. Stoevesandt and J. Peinke, Optimization of Airfoils Using the Adjoint Approach and the Influence of Adjoint Turbulent Viscosity, *Computation*, Vol. **6**, 2018.

[7] T. Verstraete and F. Coletti and B. Jérémy and T. Vanderwielen and T. Arts, Optimization of a U-Bend for Minimal Pressure Loss in Internal Cooling Channels — Part I: Numerical Method, *Journal of Turbomachinery*, Vol. **135**, 2013.

[8] K. Goc and O. Lehmkuhl and G. Park and S. Bose and P. Moin, Large eddy simulation of aircraft at affordable cost: A milestone in computational fluid dynamics, *Flow*, Vol. **1**, 2021.

[9] T. Verstraete, The VKI U-Bend Optimization Test Case, `https://aboutflow.sems.qmul.ac.uk/events/munich2016/benchmark/testcase1/`, 2016

[10] N. Gourdain and L. Gicquel and M. Montagnac and O. Vermorel and M. Gazaix and G. Staffelbach and M. Garcia and J. Boussuge and T. Poinsot, High performance parallel computing of flows in complex geometries: I. methods., *Comput. Sci. Discov.*, Vol. **2**, 2009.

[11] O. Colin and M. Rudgyard, Development of high-order Taylor-Galerkin schemes for LES, *J. Comput. Phys.*, Vol. **162**, 2000.

[12] O. Colin, A Finite Element Operator for Diffusion Terms in AVBP, *Technical Report-Institut Franais du Ptrole*, France, 2003

[13] F. Nicoud and H. B. Toda and O. Cabrit and S. Bose and J. Lee, Using singular values to build a subgrid-scale model for large eddy simulations, *Phys. Fluids*, Vol. **23**, 2011.

[14] P. Schmitt and T. Poinsot and B. Schuermans and K. Geigle, Large-eddy simulation and experimental study of heat transfer, nitric oxide emissions and combustion instability in a swirled turbulent high-pressure burner, *J. Fluid Mech.*, Vol. **570**, 2007.

[15] T. Poinsot and S. Lele, Boundary conditions for direct simulations of compressible viscous flows, *J. Comput. Phys.*, Vol. **101**, 1992.

[16] R. Fransen, LES based aerothermal modeling of turbine blade cooling systems, *Ph.D thesis, Institut National Polytechnique de Toulouse-INPT*, 2013.

[17] P. R. Spalart and S. R. Allmaras, A one equation turbulence model for aerodynamic flows, *AIAA Journal*, Vol. **92**, 1992.

[18] A. P. Singh and K. Duraisamy, Using field inversion to quantify functional errors in turbulence closures, *Physics of Fluids*, Vol. **28**, 2016.

[19] M. L. Shur and M. K. Strelets and A. K. Travin and P. R. Spalart, Turbulence Modeling in Rotating and Curved Channels: Assessing the Spalart-Shur Correction, *AIAA Journal*, Vol. **38**, 2000.

[20] F. Coletti and T. Verstraete and J. Bulle and T. Van der Wielen and N. Van den Berge and T. Arts , Optimization of a U-Bend for Minimal Pressure Loss in Internal Cooling Channels—Part II: Experimental Validation , *Journal of Turbomachinery*, Vol. **135**, 2013.

[21] F. Nicoud and F. Ducros, Subgrid-scale stress modelling based on the square of the velocity gradient tensor, *Flow, Turbulence and Combustion*, Vol. **62**, 1999.

[22] S. Auriemma, Development of parametric CAD models for gradient-based aerodynamic shape optimisation., *Ph.D thesis- Queen Mary University of London*, 2021